PHYSICAL REVIEW B **92**, 140403(R) (2015)

Competing spin-liquid states in the spin-$\frac{1}{2}$ Heisenberg model on the triangular lattice

Wen-Jun Hu, Shou-Shu Gong,* Wei Zhu, and D. N. Sheng
Department of Physics and Astronomy, California State University, Northridge, California 91330, USA
(Received 10 April 2015; revised manuscript received 7 August 2015; published 2 October 2015)

We study the spin-$\frac{1}{2}$ Heisenberg model on the triangular lattice with antiferromagnetic first- (J_1) and second- (J_2) nearest-neighbor interactions using density matrix renormalization group. By studying the spin correlation function, we find a 120° magnetic order phase for $J_2 \lesssim 0.07J_1$ and a stripe antiferromagnetic phase for $J_2 \gtrsim 0.15J_1$. Between these two phases, we identify a spin-liquid region characterized by exponential decaying spin and dimer correlations, as well as large spin singlet and triplet excitation gaps on finite-size systems. We find two near degenerating ground states with distinct properties in two sectors, which indicates more than one spin-liquid candidate in this region. While the sector with spinons is found to respect time reversal symmetry, the even sector without spinons breaks such a symmetry for finite-size systems. Furthermore, we detect the signature of the fractionalization by following the evolution of different ground states with inserting spin flux into the cylinder system. Moreover, by tuning the anisotropic bond coupling, we explore the nature of the spin-liquid phase and find the optimal parameter region for gapped Z_2 spin liquids.

DOI: 10.1103/PhysRevB.92.140403 PACS number(s): 75.10.Kt, 75.10.Jm

Quantum spin liquids (SLs) are long-range entangled states with remarkable properties of fundamental importance [1]. The SL physics has been considered to be essential to understand strongly correlated systems and unconventional superconductivity [2,3]. The simplest and perhaps most striking SLs are the gapped topological SLs, which develop a topological order [4–6] with emergent fractionalized quasiparticles [7–9]. Although SLs have been studied intensively for two decades and have been demonstrated in contrived models [10–20], the microscopic condition for the emergence of SLs in frustrated magnetic systems is not well understood.

At the experimental side, possible SLs have been discovered in various materials. Among these materials, the most promising systems are kagome antiferromagnets, including herbertsmithite and kapellasite [21–25], as well as organic Mott insulators with a triangular lattice structure such as κ-$(ET)_2Cu_2(CN)_3$ [26–29] and $EtMe_3Sb[Pd(dmit)_2]_2$ [30,31]. In all these materials, no magnetic order is observed at a temperature much lower than the interaction energy scale. These experimental findings have inspired intensive theoretical studies on frustrated magnetic systems.

Theoretically, the kagome Heisenberg model appears to possess a robust SL. Density matrix renormalization group (DMRG) studies suggest a gapped Z_2 SL [32–35]. Variational studies based on projected fermionic parton wave functions, however, favor a gapless Dirac SL [36–38]. Interestingly, by introducing second- and third-neighbor couplings [39–41] or chiral interactions [42], DMRG [40–42] studies recently discovered another topological SL, the chiral spin liquid (CSL) [43,44], which breaks time reversal symmetry (TRS) spontaneously and is identified as the $\nu = 1/2$ bosonic fractional quantum Hall state. On the other hand, the nonmagnetic phases in frustrated honeycomb and square J_1-J_2 models appear to be conventional valence-bond solid states [45–48].

The spin-$\frac{1}{2}$ triangular nearest-neighbor (NN) antiferromagnetic (AF) Heisenberg model was the first candidate proposed to realize a SL [2], although it turns out to exhibit a 120° AF order [49–53]. To understand triangular weak Mott insulator materials, combined theoretical and numerical studies [54–56] on a spin model with four-site ring-exchange couplings [57] find a gapless *spin Bose metal*. To enhance frustration [58–68], one way is to include the second-neighbor coupling J_2, where a stripe ordered state is found with larger J_2 coupling [58,59], and an intermediate nonmagnetic region may emerge [60–63]. The variational Monte Carlo simulations find a nodal d-wave SL [61] and a gapless SL [62] as candidates for this intermediate phase. Very recently, a DMRG work [69] found an indication of a gapped SL with TRS in the nonmagnetic phase. However, the nature of this intermediate phase remains far from clear.

In this Rapid Communication, we study a spin-$\frac{1}{2}$ triangular model with AF first- and second-nearest-neighbor $J_1(J_1')$-J_2 couplings using DMRG. The Hamiltonian is given as

$$H = J_1 \sum_{\langle i,j\rangle_{\text{vertical}}} \vec{S}_i \cdot \vec{S}_j + J_1' \sum_{\langle i,j\rangle_{\text{zigzag}}} \vec{S}_i \cdot \vec{S}_j + J_2 \sum_{\langle\langle i,j\rangle\rangle} \vec{S}_i \cdot \vec{S}_j,$$

where the sums $\langle i,j\rangle$ and $\langle\langle i,j\rangle\rangle$ run over all the first- and second-neighbor bonds, respectively. The first-neighbor couplings J_1 and J_1' are for the vertical and zigzag bonds, as shown in Fig. 1(a). We study most systems with $J_1' = J_1$ unless we specify otherwise. We set $J_1 = 1$ as the energy scale. By studying spin correlations, we find a nonmagnetic region sandwiched by a 120° AF phase with three sublattices for $J_2 \lesssim 0.07$ and a stripe AF phase for $J_2 \gtrsim 0.15$, as shown in Fig. 1. In this nonmagnetic region, we identify two ground states with distinct properties in two sectors, indicating two competing candidates for SL phases. The spin and dimer correlations decay exponentially with small correlation lengths. Interestingly, the chiral correlations decay exponentially fast in the odd sector with an edge spinon, while they develop long-range correlations in the even sector (with no spinon) for finite-size systems, consistent with the level crossing between two SLs for systems with different boundaries. A fractionalized spinon is detected through adiabatically inserting the spin flux. While the state in the odd sector agrees with a TRS preserving SL, the

*shoushu.gong@gmail.com

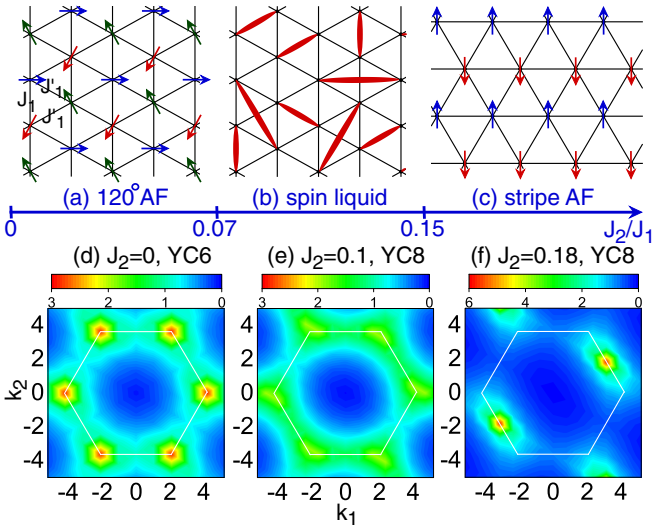

FIG. 1. (Color online) Quantum phase diagram of the isotropic spin-$\frac{1}{2}$ J_1-J_2 Heisenberg model on a triangular lattice ($J_1 = J_1'$). With growing J_2, the system has a 120° AF phase for $J_2 \lesssim 0.07$, a stripe AF phase for $J_2 \gtrsim 0.15$, and a SL phase in between. The schematic figures of the different phases also show the (a), (b) YC and (c) XC cylinder geometries. (d)–(f) are the contour plots of the spin structure factor for each phase.

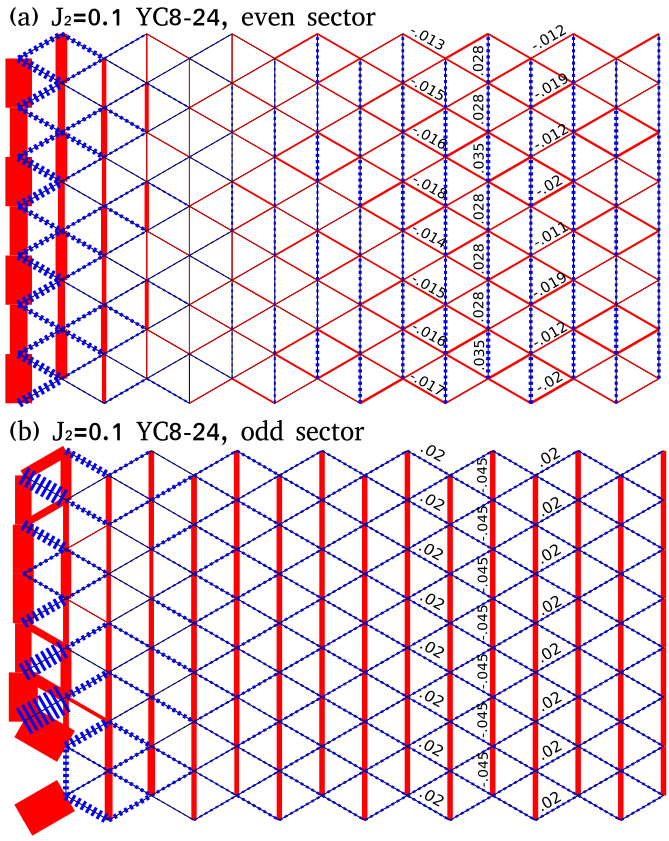

FIG. 2. (Color online) The NN bond energy $\langle S_i \cdot S_j \rangle$ for $J_2 = 0.1$ on the YC8-24 cylinder in (a) the even and (b) the odd sector. The left 16 columns are shown here. The odd sector is obtained by removing one site in each boundary of the cylinder. In both figures, all the bond energies have subtracted the average value of -0.18. The red solid and blue dashed bonds denote the negative and positive bond energies after subtraction (with some numbers shown for clarity).

TRS breaking SL (e.g., CSL) may be a competing or nearby state in more extended parameter space. Moreover, a strong bond anisotropy is observed for some finite-size systems, which may imply a nematic Z_2 SL [70]. This possible Z_2 SL is observed to be stabilized by a small bond coupling anisotropy ($J_1' \gtrsim J_1$), which suppresses chiral order in both sectors.

We study the cylinder systems using accurate $SU(2)$ DMRG [71,72] for most of the calculations and $U(1)$ DMRG [71] for inserting the flux [40]. Two cylinder geometries known as XC and YC are studied, which have one lattice direction parallel to the x or y axis, as shown in Fig. 1. We denote them as XCL_y-L_x (YCL_y-L_x), where L_y and L_x are the number of sites along the y and x directions, respectively. We study cylinder systems with L_y up to ten lattice spacings by keeping up to 20 000 $U(1)$-equivalent states in $SU(2)$ DMRG and 5000 states for inserting the flux. The truncation errors are less than 10^{-5} in all calculations, which leads to accurate results.

Even and odd topological sectors. Based on the resonating valence-bond picture, the ground states of SL on a cylinder can be either in the even or odd sector according to the parity of the number of bonds cut by a vertical line along the enclosed direction. Usually, the odd sector can be obtained by removing or adding one site on each open edge, which has been used successfully to find different sectors of the gapped SLs in kagome systems [33,73,74].

By tuning the boundary condition, we always find two different sectors on YC cylinders ($L_y = 6,8,10$), which are shown in Fig. 2 for the YC8 cylinder as an example (see the Supplemental Material for the YC10 cylinder) [75]. We find that the two sectors have the different bond energy distributions in the bulk of the cylinder. While the vertical bonds are weaker in the even sector, they become stronger in the odd sector. The nematic order, which is defined as the difference between the strong and weak bonds, exhibits distinct behaviors for the two states on the studied systems. While the nematic order grows with increased cylinder width in the odd sector, it decreases in the even sector [75].

Characteristic properties of different SL states. Next, we further characterize the two states by studying correlation functions. In Fig. 3, we show the spin correlations and dimer correlations $D_{(ij),(kl)} = \langle (S_i \cdot S_j)(S_k \cdot S_l) \rangle - \langle S_i \cdot S_j \rangle \langle S_k \cdot S_l \rangle$ for $J_2 = 0.1$, which all decay faster with growing cylinder width in both states, indicating vanishing orders in both states. Interestingly, the states in the odd sector have very short correlation lengths that are almost independent of the system width. But in the even sector, the correlation lengths are longer than those in the odd sector for the smaller $L_y = 6$ and 8, which decrease with growing system width.

To study possible TRS breaking, we calculate the scalar chiral correlation function $\langle \chi_i \chi_j \rangle$ [$\chi_i = (S_{i,1} \times S_{i,2}) \cdot S_{i,3}$]. In both sectors, the chiral order in the up and down triangles has the same direction. As shown in Fig. 3(c), in the odd sector, the chiral correlations decay quite fast and vanish. However, the chiral order and spontaneous TRS breaking are robust for the $L_y = 6,8$ systems in the even sector at

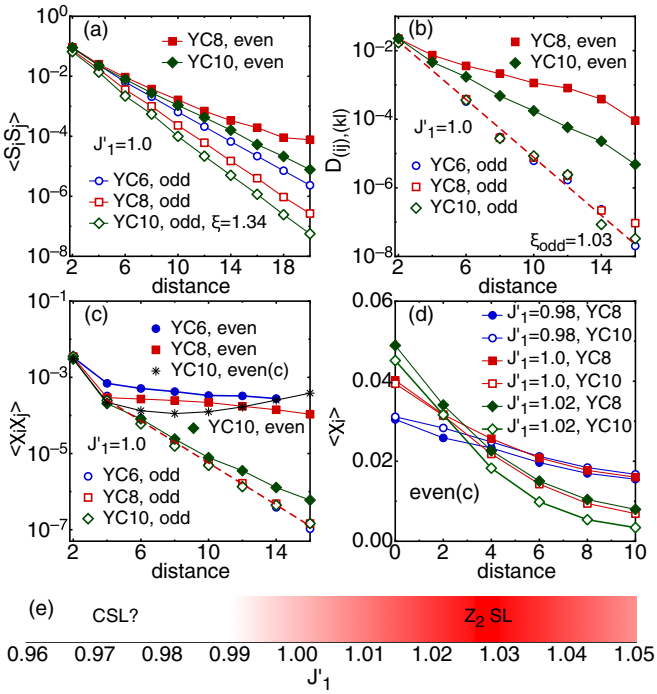

FIG. 3. (Color online) (a) and (b) are the spin and dimer correlation functions on different YC cylinders for $J_2 = 0.1$. ξ denotes the corresponding correlation lengths on the YC10 cylinder in the odd sector. (c) Chiral correlations for $J_2 = 0.1$ on different cylinders. All the data are obtained from real number DMRG calculations except "YC10, even (c)," which denotes the data obtained from complex wave function DMRG calculations on the YC10 cylinder in the even sector. (d) Chiral order from the boundary to the bulk for the bond anisotropic system in the even sector, which is obtained from the complex DMRG. (e) Schematic phase diagram for the bond anisotropic system at $J_2 = 0.1$.

the intermediate phase. As we increase the system width to $L_y = 10$, the chiral correlation becomes less robust, where different results are obtained depending on if we use complex or real initial wave functions in the DMRG simulation. The chiral correlation remains long ranged in the complex wave

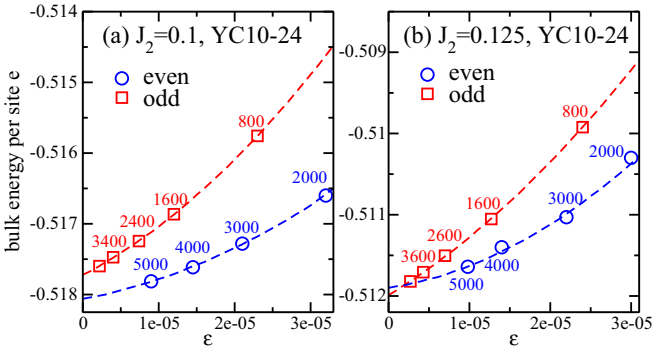

FIG. 4. (Color online) Bulk energy per site e vs DMRG truncation error ε for ground states in the even and odd sectors for (a) $J_2 = 0.1$ and (b) $J_2 = 0.125$ on the YC10-24 cylinder. The numbers denote the kept $SU(2)$ states. The energy data are fitted using the formula $e(\varepsilon) = e(0) + a\varepsilon + b\varepsilon^2$.

TABLE I. The bulk energy per site in the even (e_{even}) and odd (e_{odd}) sectors, the energy difference $\Delta e = e_{\text{even}} - e_{\text{odd}}$, and the spin triplet ($\Delta_{\text{T}}$) and singlet ($\Delta_{\text{S}}$) gaps in the odd sector for $J_2 = 0.1$ and 0.125 on the YCL_y ($L_y = 6,8,10$) cylinders. We use the fully converged results for $L_y = 6$ and 8, and the extrapolated results for $L_y = 10$ as shown in Fig. 4.

J_2, YCL_y	e_{even}	e_{odd}	Δe	Δ_{T}	Δ_{S}
0.1, YC6	−0.5155	−0.5210	0.0055	0.365	0.30
0.1, YC8	−0.5171	−0.5195	0.0024	0.335	0.26
0.1, YC10	−0.5181(2)	−0.5177	−0.0004(2)	0.30(1)	0.18
0.125,YC6	−0.5104	−0.5145	0.0041	0.389	0.33
0.125, YC8	−0.5115	−0.5133	0.0018	0.343	0.22
0.125, YC10	−0.5119(2)	−0.5120	0.0001(2)	0.30(1)	0.15

function. However, if we use a real number wave function, the DMRG will find a state with short-range chiral correlations (the real state has near identical bulk energy as the complex state but higher energy near the edge).

To further clarify the chiral order, we consider a bond anisotropy perturbation by tuning the nearest-neighbor zigzag bond as J_1' [see Fig. 1(a)]. For $J_2 = 0.1$, we find the SL persisting for $0.95 < J_1' < 1.05$. In the odd sector, all the properties are consistent with $J_1' = 1.0$. In the even sector, the chiral order appears stronger for $0.95 < J_1' \lesssim 0.99$, where it grows a bit from the YC8 to YC10 cylinder [see Fig. 3(d)]. For $J_1' \gtrsim 1.0$, the chiral order decays relatively quickly from the boundary to the bulk, especially for the larger YC10 cylinder, which indicates a possible vanishing of the chiral order in the thermodynamic limit. At $J_1' = 1.0$, the chiral correlations are strong and show long-range behavior, but the chiral order also decays with increasing system width. Thus, the two states may recover TRS at large system limits for $1.0 \lesssim J_1' < 1.05$, which is the most possible region for stabilizing a Z_2 SL. On the other hand, for $0.95 < J_1' \lesssim 0.99$, chiral order becomes stable in the even sector, while the fate of such a phase remains unclear depending on whether a chiral order would develop in a spinon sector in the thermodynamic limit. We illustrate our finding in the phase diagram [Fig. 3(e)].

We calculate the bulk ground-state energy and gaps in both sectors, which are shown in Table I for $J_2 = 0.1, 0.125$. For the smaller system widths ($L_y = 6$ and 8), the odd sectors have a lower energy than the even sectors, leading to a positive energy splitting $\Delta e = e_{\text{even}} - e_{\text{odd}}$. However, this splitting drops fast with increasing L_y, which is tiny for $L_y = 10$, indicating the close energy in both sectors. We also compute the singlet Δ_s and triplet Δ_T gaps by obtaining the ground state first and then sweeping the two low-lying states simultaneously or the $S = 1$ sector in the bulk of the cylinder [67].

Inserting flux and the nature of different sectors. Inserting flux is an effective way to identify topological properties, which has been used in DMRG to study topological SLs [40,73,74]. To introduce a flux, we impose the twist boundary condition in the y direction by replacing terms $S_i^+ S_j^- + \text{H.c.} \rightarrow S_i^+ S_j^- e^{i\theta} + \text{H.c.}$ for all neighboring bonds crossing the y boundary. We start from the even sector by adiabatically increasing θ and measuring the evolution of the spin-z local magnetization $\langle S_i^z \rangle$. With increasing θ, a net spin z accumulates on the open edges, as shown in

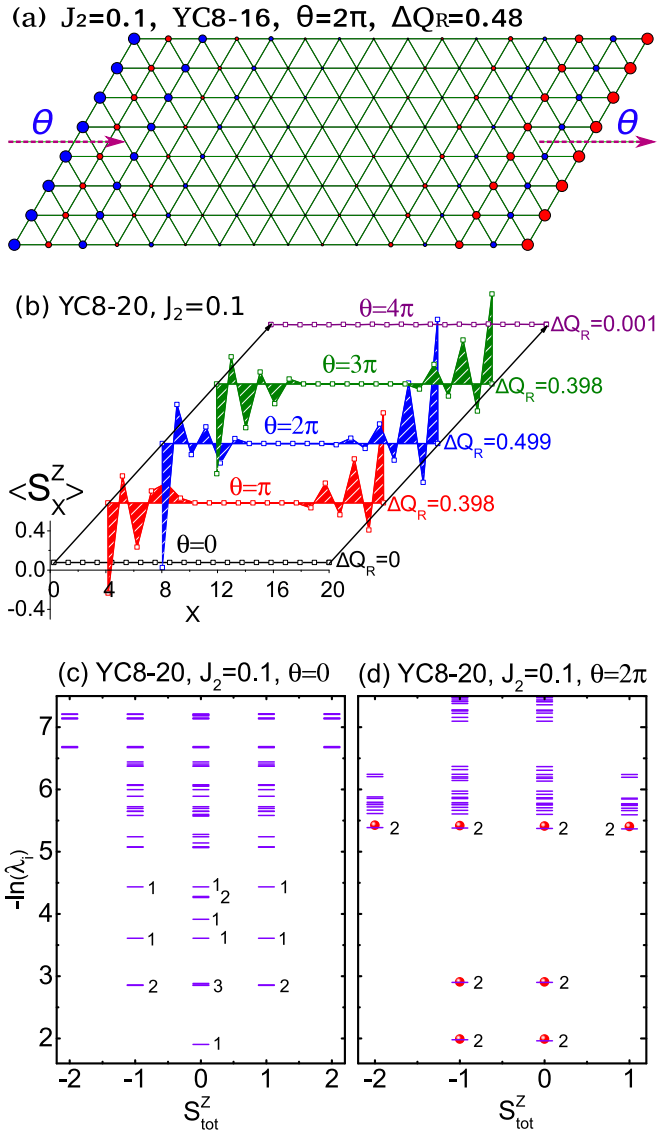

FIG. 5. (Color online) (a) Real-space configuration of spin magnetization $\langle S_i^z \rangle$ after adiabatically inserting a flux $\theta = 2\pi$. The red and blue circles denote the positive and negative $\langle S_i^z \rangle$ with the area of the circle proportional to the amplitude of $\langle S_i^z \rangle$. ΔQ_R is the net spin accumulation on the right edge $\Delta Q_R = \sum_i \langle S_i^z \rangle$, where i denotes the site on the right edge of the cylinder. (b) Real-space configuration of the accumulated spin magnetization in each column with increasing flux. Low-lying ES at the flux (c) $\theta = 0$ and (d) $\theta = 2\pi$. The numbers in ES denote the near-degenerate eigenvalues in large weight levels. At $\theta = 2\pi$ in (d), all the eigenvalues are double degenerate, as explicitly shown by the circles for the low-lying levels.

Fig. 5(a), indicating that the quasiparticle responding to the flux here must carry spin, such as the spinon in CSL [40] and the fermionic spinon (spinon bonded with vison) in Z_2 SL [73,76,77].

With the flux $\theta = 0 \to 2\pi$, the net spin grows continuously from 0 to 0.5 on the edges, as shown in Fig. 5(b). At $\theta = 2\pi$, an $S^z = \pm 1/2$ spinon develops on each boundary, and the ground state evolves to a new sector. By further increasing $\theta = 2\pi \to 4\pi$, the net spin dissipates continuously to zero, and the system evolves back to the even sector. In Figs. 5(c) and 5(d), we demonstrate the entanglement spectrum (ES) with inserting flux. At $\theta = 0$ in the even sector, the whole ES is symmetric about $S^z = 0$. At $\theta = 2\pi$, the ES becomes symmetric about $S^z = 1/2$, consistent with the fractionalized spin-carrying quasiparticles on boundaries. Interestingly, each eigenvalue of the ES at $\theta = 2\pi$ is doubly degenerate. By comparing the odd sector obtained by removing sites and the sector with flux $\theta = 2\pi$ here, we find that these two states have the same bulk energy and ES, indicating that the two sectors obtained by different methods are exactly the same. This odd sector might be consistent with the fermionic spinon sector of the Z_2 SL [76–78].

Summary and discussions. By means of DMRG calculations on wide cylinder systems of the spin-$\frac{1}{2}$ J_1-J_2 Heisenberg model on a triangular lattice, we find a SL region bordered by a 120° Néel AF phase for $J_2 \lesssim 0.07$ and a stripe AF phase for $J_2 \gtrsim 0.15$. The spin and dimer correlations all decay fast for wider systems with small correlation lengths comparable to lattice constants with large spin and singlet excitation gaps. The ES in the odd sector could be consistent with the fermionic spinon in Z_2 SL. However, the long-range chiral correlation is observed in the even sector for a space isotropic model. By tuning the anisotropic bond coupling, we find that the possible gapped Z_2 SL is stabilized by some weak anisotropy ($J_1' \sim 1.02$). The chiral correlations are enhanced in the even sector by opposite anisotropy ($J_1' \sim 0.98$), which may be stabilized in both sectors by TRS breaking terms, and we leave this open issue for future studies.

Note added. Recently, we became aware of some related papers [69,79]. We reached a similar conclusion on gapped SLs with Ref. [69].

Acknowledgments. We acknowledge stimulating discussions with T. Senthil, X. G. Wen, Z. Y. Zhu, S. R. White, F. Wang, and Y. Qi. This research is supported by the National Science Foundation through Grants No. PREM DMR-1205734 (W.J.H.) and No. DMR-1408560 (S.S.G., D.N.S.), and the US Department of Energy, Office of Basic Energy Sciences under Grant No. DE-FG02-06ER46305 (W.Z.).

[1] L. Balents, Nature (London) **464**, 199 (2010).
[2] P. W. Anderson, Mater. Res. Bull. **8**, 153 (1973).
[3] P. A. Lee, N. Nagaosa, and X.-G. Wen, Rev. Mod. Phys. **78**, 17 (2006).
[4] X. G. Wen, Phys. Rev. B **40**, 7387 (1989).
[5] X. G. Wen and Q. Niu, Phys. Rev. B **41**, 9377 (1990).
[6] X.-G. Wen, Int. J. Mod. Phys. B **4**, 239 (1990).
[7] X. G. Wen, Phys. Rev. B **44**, 2664 (1991).
[8] T. Senthil and M. P. A. Fisher, Phys. Rev. B **62**, 7850 (2000).
[9] T. Senthil and M. P. A. Fisher, Phys. Rev. Lett. **86**, 292 (2001).
[10] D. S. Rokhsar and S. A. Kivelson, Phys. Rev. Lett. **61**, 2376 (1988).

[11] N. Read and S. Sachdev, Phys. Rev. Lett. **66**, 1773 (1991).
[12] R. Moessner and S. L. Sondhi, Phys. Rev. Lett. **86**, 1881 (2001).
[13] L. Balents, M. P. A. Fisher, and S. M. Girvin, Phys. Rev. B **65**, 224412 (2002).
[14] T. Senthil and O. Motrunich, Phys. Rev. B **66**, 205104 (2002).
[15] O. I. Motrunich and T. Senthil, Phys. Rev. Lett. **89**, 277004 (2002).
[16] D. N. Sheng and L. Balents, Phys. Rev. Lett. **94**, 146805 (2005).
[17] A. Kitaev, Ann. Phys. (NY) **321**, 2 (2006).
[18] H. Yao and S. A. Kivelson, Phys. Rev. Lett. **99**, 247203 (2007).
[19] D. F. Schroeter, E. Kapit, R. Thomale, and M. Greiter, Phys. Rev. Lett. **99**, 097202 (2007).
[20] S. V. Isakov, M. B. Hastings, and R. G. Melko, Nat. Phys. **7**, 772 (2011).
[21] P. Mendels, F. Bert, M. A. de Vries, A. Olariu, A. Harrison, F. Duc, J. C. Trombe, J. S. Lord, A. Amato, and C. Baines, Phys. Rev. Lett. **98**, 077204 (2007).
[22] J. S. Helton, K. Matan, M. P. Shores, E. A. Nytko, B. M. Bartlett, Y. Yoshida, Y. Takano, A. Suslov, Y. Qiu, J.-H. Chung *et al.*, Phys. Rev. Lett. **98**, 107204 (2007).
[23] M. A. de Vries, J. R. Stewart, P. P. Deen, J. O. Piatek, G. J. Nilsen, H. M. Rønnow, and A. Harrison, Phys. Rev. Lett. **103**, 237201 (2009).
[24] B. Fåk, E. Kermarrec, L. Messio, B. Bernu, C. Lhuillier, F. Bert, P. Mendels, B. Koteswararao, F. Bouquet, J. Ollivier *et al.*, Phys. Rev. Lett. **109**, 037208 (2012).
[25] T.-H. Han, J. S. Helton, S. Chu, D. G. Nocera, J. A. Rodriguez-Rivera, C. Broholm, and Y. S. Lee, Nature (London) **492**, 406 (2012).
[26] Y. Shimizu, K. Miyagawa, K. Kanoda, M. Maesato, and G. Saito, Phys. Rev. Lett. **91**, 107001 (2003).
[27] Y. Kurosaki, Y. Shimizu, K. Miyagawa, K. Kanoda, and G. Saito, Phys. Rev. Lett. **95**, 177001 (2005).
[28] S. Yamashita, Y. Nakazawa, M. Oguni, Y. Oshima, H. Nojiri, Y. Shimizu, K. Miyagawa, and K. Kanoda, Nat. Phys. **4**, 459 (2008).
[29] M. Yamashita, N. Nakata, Y. Kasahara, T. Sasaki, N. Yoneyama, N. Kobayashi, S. Fujimoto, T. Shibauchi, and Y. Matsuda, Nat. Phys. **5**, 44 (2009).
[30] T. Itou, A. Oyamada, S. Maegawa, M. Tamura, and R. Kato, Phys. Rev. B **77**, 104413 (2008).
[31] M. Yamashita, N. Nakata, Y. Senshu, M. Nagata, H. M. Yamamoto, R. Kato, T. Shibauchi, and Y. Matsuda, Science **328**, 1246 (2010).
[32] H. C. Jiang, Z. Y. Weng, and D. N. Sheng, Phys. Rev. Lett. **101**, 117203 (2008).
[33] S. Yan, D. A. Huse, and S. R. White, Science **332**, 1173 (2011).
[34] S. Depenbrock, I. P. McCulloch, and U. Schollwöck, Phys. Rev. Lett. **109**, 067201 (2012).
[35] H.-C. Jiang, Z. Wang, and L. Balents, Nat. Phys. **8**, 902 (2012).
[36] Y. Ran, M. Hermele, P. A. Lee, and X.-G. Wen, Phys. Rev. Lett. **98**, 117205 (2007).
[37] Y. Iqbal, F. Becca, S. Sorella, and D. Poilblanc, Phys. Rev. B **87**, 060405 (2013).
[38] Y. Iqbal, D. Poilblanc, and F. Becca, Phys. Rev. B **89**, 020407 (2014).
[39] L. Messio, B. Bernu, and C. Lhuillier, Phys. Rev. Lett. **108**, 207204 (2012).
[40] S.-S. Gong, W. Zhu, and D. Sheng, Sci. Rep. **4**, 6317 (2014).
[41] Y.-C. He, D. N. Sheng, and Y. Chen, Phys. Rev. Lett. **112**, 137202 (2014).
[42] B. Bauer, L. Cincio, B. P. Keller, M. Dolfi, G. Vidal, S. Trebst, and A. W. W. Ludwig, Nat. Commun. **5**, 5137 (2014).
[43] V. Kalmeyer and R. B. Laughlin, Phys. Rev. Lett. **59**, 2095 (1987).
[44] X. G. Wen, F. Wilczek, and A. Zee, Phys. Rev. B **39**, 11413 (1989).
[45] R. Ganesh, J. van den Brink, and S. Nishimoto, Phys. Rev. Lett. **110**, 127203 (2013).
[46] Z. Zhu, D. A. Huse, and S. R. White, Phys. Rev. Lett. **110**, 127205 (2013).
[47] S.-S. Gong, D. N. Sheng, O. I. Motrunich, and M. P. A. Fisher, Phys. Rev. B **88**, 165138 (2013).
[48] S.-S. Gong, W. Zhu, D. N. Sheng, O. I. Motrunich, and M. P. A. Fisher, Phys. Rev. Lett. **113**, 027201 (2014).
[49] S. Sachdev, Phys. Rev. B **45**, 12377 (1992).
[50] B. Bernu, C. Lhuillier, and L. Pierre, Phys. Rev. Lett. **69**, 2590 (1992).
[51] L. Capriotti, A. E. Trumper, and S. Sorella, Phys. Rev. Lett. **82**, 3899 (1999).
[52] W. Zheng, J. O. Fjærestad, R. R. P. Singh, R. H. McKenzie, and R. Coldea, Phys. Rev. B **74**, 224420 (2006).
[53] S. R. White and A. L. Chernyshev, Phys. Rev. Lett. **99**, 127004 (2007).
[54] O. I. Motrunich, Phys. Rev. B **72**, 045105 (2005).
[55] D. N. Sheng, O. I. Motrunich, and M. P. A. Fisher, Phys. Rev. B **79**, 205112 (2009).
[56] M. S. Block, R. V. Mishmash, R. K. Kaul, D. N. Sheng, O. I. Motrunich, and M. P. A. Fisher, Phys. Rev. Lett. **106**, 046402 (2011).
[57] G. Misguich, C. Lhuillier, B. Bernu, and C. Waldtmann, Phys. Rev. B **60**, 1064 (1999).
[58] T. Jolicoeur, E. Dagotto, E. Gagliano, and S. Bacci, Phys. Rev. B **42**, 4800 (1990).
[59] A. V. Chubukov and T. Jolicoeur, Phys. Rev. B **46**, 11137 (1992).
[60] L. O. Manuel and H. A. Ceccatto, Phys. Rev. B **60**, 9489 (1999).
[61] R. V. Mishmash, J. R. Garrison, S. Bieri, and C. Xu, Phys. Rev. Lett. **111**, 157203 (2013).
[62] R. Kaneko, S. Morita, and M. Imada, J. Phys. Soc. Jpn. **83**, 093707 (2014).
[63] P. H. Y. Li, R. F. Bishop, and C. E. Campbell, Phys. Rev. B **91**, 014426 (2015).
[64] S. Yunoki and S. Sorella, Phys. Rev. B **74**, 014408 (2006).
[65] M. Q. Weng, D. N. Sheng, Z. Y. Weng, and R. J. Bursill, Phys. Rev. B **74**, 012407 (2006).
[66] O. A. Starykh, H. Katsura, and L. Balents, Phys. Rev. B **82**, 014421 (2010).
[67] A. Weichselbaum and S. R. White, Phys. Rev. B **84**, 245130 (2011).
[68] K. Li, S.-L. Yu, and J.-X. Li, New J. Phys. **17**, 043032 (2015).
[69] Z. Zhu and S. R. White, Phys. Rev. B **92**, 041105 (2015).
[70] K. Slagle and C. Xu, Phys. Rev. B **89**, 104418 (2014).
[71] S. R. White, Phys. Rev. Lett. **69**, 2863 (1992).
[72] I. McCulloch and M. Gulácsi, Europhys. Lett. **57**, 852 (2002).
[73] Y.-C. He, D. N. Sheng, and Y. Chen, Phys. Rev. B **89**, 075110 (2014).

[74] W. Zhu, S. Gong, and D. Sheng, J. Stat. Mech.: Theory Exp. (2014) P08012.
[75] See Supplemental Material at http://link.aps.org/supplemental/10.1103/PhysRevB.92.140403 for more details.
[76] Y. Qi and L. Fu, Phys. Rev. B **91**, 100401 (2015).
[77] M. Zaletel, Y.-M. Lu, and A. Vishwanath, arXiv:1501.01395.
[78] M. P. Zaletel and A. Vishwanath, Phys. Rev. Lett. **114**, 077201 (2015).
[79] S. N. Saadatmand, B. J. Powell, and I. P. McCulloch, Phys. Rev. B **91**, 245119 (2015).